International Journal of Mass Spectrometry 283 (2009) 149–160

Contents lists available at ScienceDirect

International Journal of Mass Spectrometry

journal homepage: www.elsevier.com/locate/ijms

Developing IMS–IMS–MS for rapid characterization of abundant proteins in human plasma

Stephen J. Valentine[a,*], Ruwan T. Kurulugama[a], Brian C. Bohrer[a], Samuel I. Merenbloom[a], Renã A. Sowell[b], Yehia Mechref[a], David E. Clemmer[a,*]

[a] Department of Chemistry, Indiana University, Bloomington, IN 47405, United States
[b] Department of Chemistry, University of Kentucky, Lexington, KY 40506, United States

ARTICLE INFO

Article history:
Received 27 December 2008
Received in revised form 24 February 2009
Accepted 25 February 2009
Available online 24 March 2009

Keywords:
Ion mobility spectrometry
Proteomics
Multidimensional IMS

ABSTRACT

A drift tube mass spectrometer that utilizes back-to-back ion mobility regions separated by a collisional activation zone and new autosampling [R.T. Kurulugama, S.J. Valentine, R.A. Sowell, D.E. Clemmer, Development of a high-throughput IMS–IMS–MS approach for analyzing mixtures of biomolecules, J. Proteomics 71 (3) (2008) 318–331] and data acquisition techniques [S. Trimpin, D.E. Clemmer, Ion mobility spectrometry/mass spectrometry snapshots for assessing the molecular compositions of complex polymeric systems, Anal. Chem. 80 (23) (2008) 9073–9083; C. Becker, K.N. Qian, D.H. Russell, Molecular weight distributions of asphaltenes and deasphaltened oils studied by laser desorption ionization and ion mobility mass spectrometry, Anal. Chem. 80 (22) (2008) 8592–8597; S.I. Merenbloom, S.L. Koeniger, B.C. Bohrer, S.J. Valentine, D.E. Clemmer, Improving the efficiency of IMS–IMS by a combing technique, Anal. Chem. 80 (6) (2008) 1918–1927; M.E. Belov, B.H. Clowers, D.C. Prior, W.F. Danielson III, A.V. Liyu, B.O. Petritis, R.D. Smith, Dynamically multiplexed ion mobility time-of-flight mass spectrometry, Anal. Chem. 80 (15) (2008) 5873–5883] is used to analyze tryptic peptides from proteins obtained from 70 individual human plasma samples. The combination of methods allows ions to be efficiently separated in an initial drift region (based on differences in mobilities that arise from initial conformations), activated (in order to alter conformations), and then separated again in a second drift region, prior to detection in a mass spectrometer. The two-dimensional ion mobility separation makes it possible to create a large analytical peak capacity for the complex mixture. Additionally, the mobility distributions of the ions in different states (precursor and post-activation) provide a signature that is valuable in verifying that the same ions are being examined across the distribution of individuals. Finally, because this characterization is carried out in the gas phase it is possible to obtain information in a high-throughput fashion. Here, we develop and assess an analysis that requires ~4 min per sample. While this prototype approach is at a very early stage several thousand peaks can be resolved and detected for each sample. From a comparison of 15 plasma samples analyzed with IMS–IMS–MS and LC–MS/MS techniques we find that an average of 262 ± 54 (1σ) unique peptides assigned in the latter analyses are also observed in the former. On average, these assigned peptides represent 63 ± 9 proteins. The utility of the approach as a means of characterizing physiologies in a state-to-state fashion is discussed.

1. Introduction

In 1991 Kemper and Bowers separated different electronic states of transition metals in a drift tube based on differences in their mobilities through He buffer gas [1–3]. They went on to propose that under certain conditions it is possible to follow transitions, from one electronic state to another using this technique [3]. Subsequently, reliable methods for calculating mobilities [4–7] for atomic coordinates generated by theory were developed to provide direct structural information for a range of different systems, such as metal coordination complexes [8–12], synthetic polymers [9,11,13–19], clusters [20–25], and biopolymers [8,10,26–37], The structural insight accessible from this approach attracted considerable attention. An early example was the family of rings and fullerenes that were produced upon laser vaporization of carbon rods [38–41]. This noted structural determination is only one of many uses for drift tubes. These instruments are well suited for studying gas-phase chemical reactivity under thermal conditions

* Corresponding authors.
E-mail address: clemmer@indiana.edu (D.E. Clemmer).

1387-3806/$ – see front matter © 2009 Published by Elsevier B.V.
doi:10.1016/j.ijms.2009.02.030

[39,2,20,42] as well as state-to-state studies that involve non-reactive changes in structure [43,44] that can be resolved as a difference in mobility. Currently, the techniques are employed for a range of different studies, from understanding how electrons rearrange in atoms [3], to assessing how peptides aggregate [45–47], as well as how protein complexes assemble and dissociate [48–51]; and this list does not include more traditional applications (e.g., particle sizing [52] and chemical warfare agent and explosives detection [53,54]).

Recently our group coupled two- and three-dimensional ion mobility spectrometry (IMS–IMS and IMS–IMS–IMS) techniques with time-of-flight mass spectrometry (MS) in order to realize large analytical peak capacities that would facilitate separation of large mixtures of molecules as they emerge from an ion source [55–58]. In this approach, we separate ions in a first drift region, expose them to energizing collisions in order to induce structural changes, and then separate the mixture again based on the new structures that are formed. IMS–IMS and IMS–IMS–IMS techniques also are suitable for following changes in conformations of ions—from defined precursor states (i.e., a distribution of ions with identical mobilities), through selected intermediates to product states [43,44].

The longer term goal of the work to develop this technology has been the possibility of using the large peak capacities and defined signatures associated with transitions generated by very-high-throughput gas-phase ion techniques for state-to-state measurements at a physiological scale on living organisms. For example, consider the data in Fig. 1, which illustrate early attempts to characterize the proteome of *Drosophila melanogaster* (the fruit fly) as the population evolves over its lifetime [59]. Two examples of proteins are shown: paramyosin, which remains at a relatively constant concentration across lifespan; and prophenyloxidase which decreases dramatically in concentration as the organism ages. Prophenyloxidase (as well as other proteins) is known to be involved in the immune response mechanism for this animal. The relative concentration of this protein reflects the animals' ages, and can be used to predict the remaining lifetime of a synchronized population. Also shown are population lifespan data obtained upon deletion of this gene; the average lifespan is reduced. In other studies, single gene changes, related to diseased states suggest that cascades of events occur at the level of the proteome. For example, a Parkinson's disease mutant (A30P) of human α-synuclein protein expressed in flies leads to dramatic changes in structural proteins such as actin-associated proteins compared with control animals [60]. Using IMS–MS measurements, Bowers and his collaborators have suggested that spermine, a polyamine involved in metabolic processes, induces a structural transition in α-synuclein and the related A30P and A53T α-synuclein mutants [49]. The transition they observed involves the collapse of extended conformations to form highly compact structures which are believed to form aggregates and lead to disease onset.

At the heart of the push towards state-to-state measurements at the physiological level is a tremendous barrier—the time required to do the experiments. The fruit fly experiments described above required several years to complete, and still many issues are unresolved. Commercially available, state-of-the-art techniques are by nature time consuming (e.g., gels may require weeks for a single separation and identifications may add substantially to the total time of the experiment; chromatographic separations usually require hrs to carry out). Moreover, limitations in run-to-run and lab-to-lab measurement reproducibility (with current technologies), requires that many replicate experiments be done in order to make definitive conclusions. In the last decade many new approaches that utilize the highly controlled environment of the gas phase for rapid and sensitive analysis of complex mixtures have emerged.

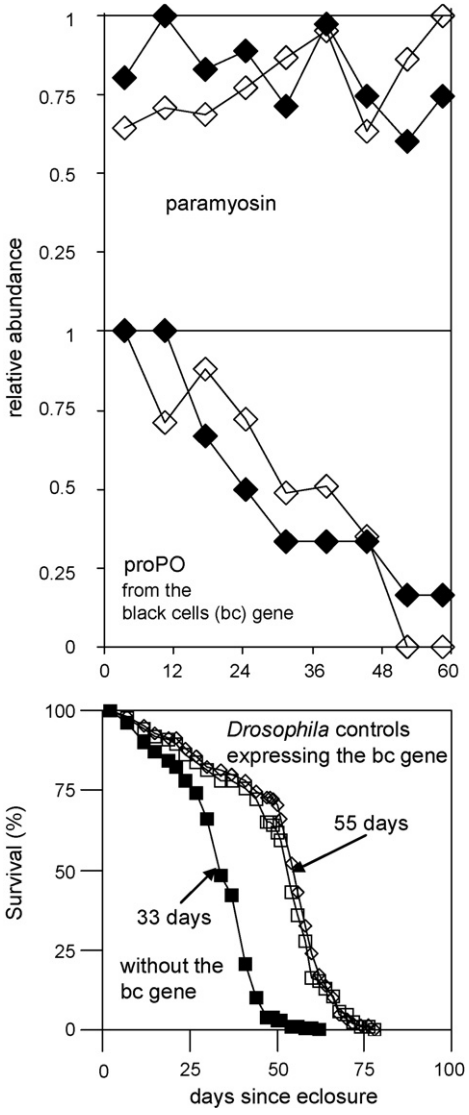

Fig. 1. The top two plots show relative protein concentrations as a function of age obtained from LC–MS/MS analyses of *Drosophila melanogaster* heads. Traces for the protein paramyosin (top plot) and for the protein prophenyloxidase (middle plot) are shown for duplicate analyses. The first data trace (solid symbols) is obtained using LC–MS/MS analyses and relative protein concentration is obtained using the peptide ion hits technique. The second data trace (open symbols) is obtained using LC–IMS–MS analyses of the same samples and relative protein concentration is obtained using peptide ion intensities. For details see Ref. [59]. The bottom plot shows survival curves for three different *D. melanogaster* genotype populations. Two heterozygous control populations are shown as open symbols while a homozygous population which lacks prophenyloxidase activity is shown as solid symbols. The population age corresponding to ~50% survival is shown for the two different genotype populations.

The experiments presented below benefit from and expand upon previous efforts to improve analytical peak capacities for complex mixture analysis using ion mobility techniques [61–67] including recent work aimed at coupling mobility separation steps [55–58,68,69,34,70]. The work described here represents the first step towards developing multiplexed IMS–IMS protocols (IMS combing) [58] for high-throughput analysis. Below, we examine the plasma proteome from 70 individuals. Because plasma is in contact (either directly or indirectly) with all of the 10^{14}–10^{15} human cells in our bodies [and perhaps as many non-human cells (e.g., those from bacteria or fungi)] [71,72] analyses before and after applied perturbations may provide insight into why various changes occur.

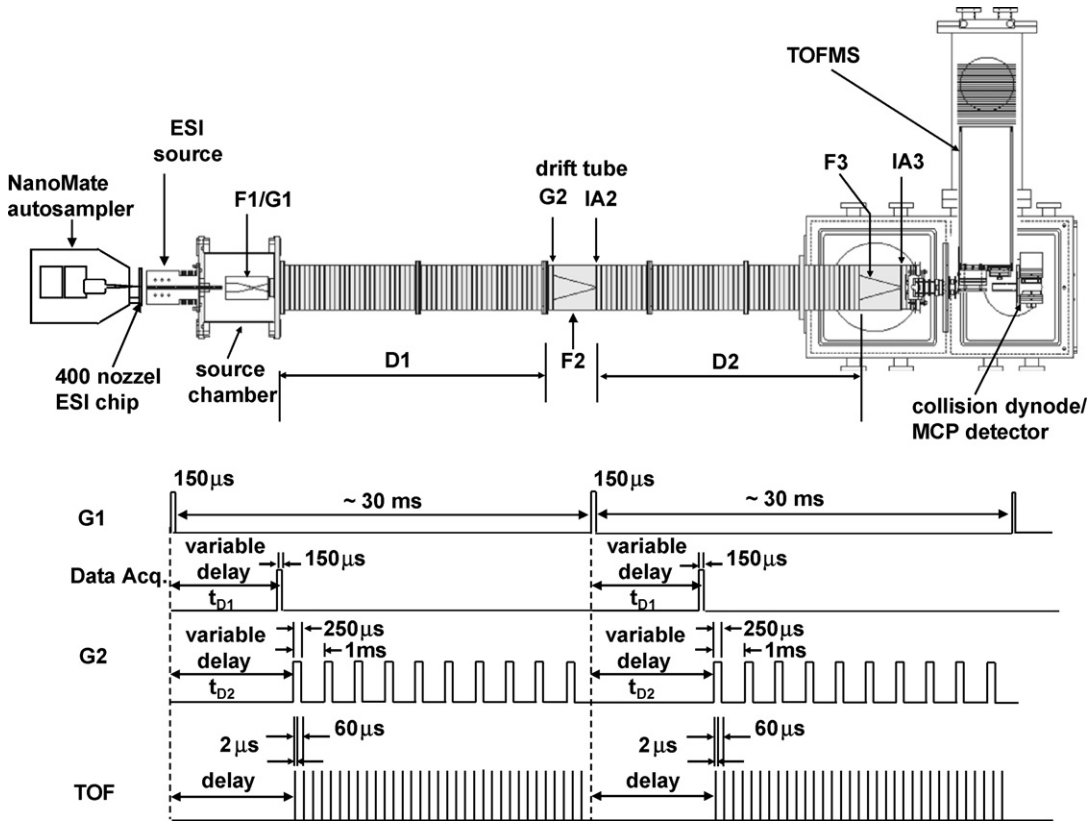

Fig. 2. Schematic of the IMS–IMS–MS instrument used in these experiments (top). Timing pulse sequence used in the IMS–IMS–MS experiments (bottom). Shown are the timing pulses applied to the instrument gates (G1 and G2), the data acquisition system, and the TOF high-voltage pulser. It is important to note that the delay times t_{D1} and t_{D2} have the relationship $t_{D2} \geq t_{D1}$. Pulse widths and periods are provided.

This is the first report of the use of IMS–IMS techniques for assessing the proteome of a large number of samples; we note that one large IMS–MS study of glycans from human plasma has been presented [73]. Our primary focus is to examine how many proteins could be followed using this approach when operated in a very-high-throughput mode. Here, the total time for analysis was chosen to be 4 min/sample.

2. Experimental

2.1. General

Fig. 2 shows a schematic of the instrument used to characterize the plasma samples. Descriptions of IMS–MS measurements [74–77], instrumentation [78–95], and theory [74,96–101] have been provided elsewhere including a recent description of the coupling of the NanoMate autosampler to an IMS–IMS–MS instrument [102]. Only a brief description of the measurement as it pertains to plasma digest analysis is presented here. A 15 μL aliquot of plasma digest sample (see below) was drawn into a new NanoMate tip and delivered to the ESI nanospray chip containing 400 nozzles. Voltage was then applied to the chip and ions were electrosprayed into the entrance orifice of the IMS instrument shown in Fig. 2. Ions were accumulated in the exit region of the first ion funnel prior to periodic extraction into the first drift region of the IMS instrument. In the drift tube ions were separated based on difference in their mobilities through an inert buffer gas (He) under the influence of an applied electric field. Ions exiting the drift tube were focused into the source region of a time-of-flight (TOF) mass spectrometer and subsequently mass analyzed. The instrument was operated using two sequential mobility separations; this method is described in detail below.

2.2. Plasma samples

Plasma samples were obtained from recruited subjects under the direction of an IRB-approved protocol.[1] Approximately 6 mL of plasma were drawn into sample tubes containing lithium heparin (Vacutainer, BD). Samples were immediately centrifuged (3000 × *g* at 5 min) to obtain plasma. The plasma was decanted into transfer tubes and stored on ice for transfer to the laboratory. Upon arrival, a protease inhibitor cocktail (Sigma–Aldrich) was introduced to each plasma sample and samples were subsequently stored at −80 °C until further analysis.

2.3. Abundant protein removal

The six most abundant proteins (albumin, IgG, IgA, serotransferrin, haptoglobin, and antitrypsin) were removed from each plasma sample using the Multiple Affinity Removal System (MARS) LC column (Agilent). Briefly, a 90-μL aliquot from each sample was diluted with Buffer A (Buffers A and B are proprietary buffers from Agilent) and subsequently filtered using a 0.22 μm spin filter (Agilent) to remove particulate matter in the plasma. The filtrate was then loaded onto the MARS LC column using a high-pressure LC (600 series pump; 2487 dual λ detector, Waters). The LC system was operated as follows: 100% Buffer A (0.5 mL min^{-1}) for 10 min and 100% B (1.0 mL min^{-1}) for 7 min. The flow-through fraction containing the lower abundance proteins was collected while washing the column with Buffer A. This fraction eluted from ~2–~5 min after start of the washing step. The bound fraction (higher abundance proteins) was collected over an elution time

[1] Study number 05-10163, Indiana University Institutional Review Board.

range of ~14–~16 min. The column was regenerated by equilibrating with Buffer A for 11 min prior to the next sample injection. The flow-through fraction was subsequently concentrated to ~300 μL using a 4.0 mL Vivaspin 5 kDa molecular weight cutoff filter (Agilent) and centrifugation. Samples were then stored at ~4 °C until protein digestion.

2.4. Plasma protein digestion

Each plasma sample (~300 μL) was diluted to 2 mL with 200 mM ammonium bicarbonate buffer (pH ~8.0) containing 6 M urea. After the denaturation step, plasma samples were reduced using a dithiothreitol stock solution (1 M in 200 mM ammonium bicarbonate) at a molar ratio of 1:40 (protein:DTT). This reaction was carried out at 37 °C. After reducing the disulfide bonds, samples were placed on ice and proteins were alkylated using iodoacetamide stock solution (1 M in 200 mM ammonium bicarbonate) at a molar ratio of 1:80 (protein:iodoacetamide). This reaction proceeded in darkness for 2 h. Next, excess Cysteine (40-fold from a 1 M in 200 mM ammonium bicarbonate stock solution) was added to the mixture to remove remaining reagent. This reaction proceeded at room temperature for 30 min Finally, the samples were diluted with 4.0 mL of 200 mM ammonium bicarbonate solution and TPCK-treated trypsin (Sigma–Aldrich) was added to the mixture (2%, wt/wt). Protein digestion was allowed to proceed for 24 h at 37 °C. The resulting tryptic peptides were desalted using Oasis HLB cartridges (Waters) and finally dried using a centrifugal concentrator (Labconco).

2.5. Electrospray solutions

Peptide digests were resuspended in 200 μL of ESI solution (49:49:2 water:methanol:acetic acid). This was accomplished by first adding 100 μL of ESI solution followed by extensive vortexing. Next the remaining 100 μL was added to each sample followed by further vortexing. Next 40 μL of each sample was introduced into a single well of the 96-well sample plate. ESI samples were batch processed in groups of 12 prior to analysis in order to maintain sample integrity. Aluminum foil with adhesive (Advion) was applied to the 96-well plate to prevent sample solution evaporation.

To each sample, 10 μL of a peptide mixture of angiotensin I and bradykinin (each 5×10^{-3} mg mL^{-1} in ESI solution) was added to provide internal standards for comparative analyses. These two peptides provide ideal internal standards for these mixtures. At the concentrations used for the studies reported here, three charge states (+1, +2, +3) are observed for both peptides. Because, collision cross sections for the respective charge states are different for the two peptides, a significant portion of the drift time range contains one of the respective peptide ions. In fact, each IMS–IMS dataset frame contains at least one of the ions. Although the selected peptide ions exist in human plasma, circulating concentrations are expected to be quite low (pg mL^{-1}) [103–105], that is, below detectable levels in this experiment where all mixture components are electrosprayed simultaneously. For a number of sensitivity studies where plasma digests have been spiked with serial dilutions of each peptide, at the detection limits (~200 attomoles), internal standard peaks are barely distinguished from the noise and working curves indicated the inability to detect the peptides below this level. Internal standard concentrations are relatively high such that any endogenous level appears to not affect the normalization step as further evidenced by the fact that normalization to total ion intensities provides similar results. That said, because sensitivity studies were not carried out for each sample, the possibility of endogenous peptides affecting the relative quantitation measurements cannot be ruled out. Future studies will utilize a tryptic digest of a non-native protein such as soybean trypsin inhibitor [106].

2.6. Multiplexed IMS–IMS–MS measurements

Two-dimensional IMS measurements can only be achieved by altering the mobility of the ion between sequential measurements. In the analysis of the plasma digest samples this was accomplished using two sequential drift regions which contain an ion selection (gate) and ion activation interface region. Fig. 2 shows a pulse timing diagram demonstrating the procedure for IMS–IMS–MS measurements. Periodically, ion packets from the first ion funnel were extracted into the first drift region for mobility separation. After a predetermined delay time (Fig. 2), the arrival times of ions (drift and TOF) were recorded with the data acquisition system. After a second predetermined delay time equal to or greater than the first, ions of a specific mobility were selected using the ion gate G2 (Fig. 2). Immediately afterward, ions were activated in the second activation region (IA2 in Fig. 2) to alter their structures. The activation conditions employed here were optimized to produce maximum structural changes in the +2 and +3 charge states of peptide ions while causing minimal ion fragmentation. Following activation, the ions internal temperature rapidly re-equilibrates to the buffer gas temperature and the new structures are then separated in the second drift region prior to MS analysis.

This activation process can be operated in a multiplexed fashion, referred to as *combing*, as described previously [58]. This is accomplished by employing multiple mobility selections within a single experimental sequence. In the present experiments, each mobility selection is 250 μs wide and spaced apart by 1 ms (referred to as the IMS comb teeth, Fig. 2) for each packet of ions introduced into the first drift region. After collecting data for a specified period of time (45 s in this case), the mobility selections were shifted by 250 μs to characterize ions of different mobilities within the original ion packet originating in the first funnel (F1 in Fig. 2). This process was repeated three times for each sample in order to examine all ions with mobiliities between the original mobility selection settings. Thus, each sample dataset contained four data frames. The first contained the mobility, m/z, and intensity information for all features observed using the original set of mobility selections. The second contained the same information for the second set of mobility selections and the same with the third and fourth data frames. A fifth data frame is not required as these mobility selections would be a repeat of the first selections (albeit shifted by 1 ms). For these studies, each data frame was collected for 45 s leading to a total time of 3 min for data collection per sample. The process of saving the data and switching samples required an additional minute and so the experimental time required for each sample was 4 min.

The TOF mass spectrometer used in the current studies has a resolving power of ~5000–~7000 for ions with mass-to-charge (m/z) of 500. This is accomplished using a TOF bin resolution of 100 ps. However, for data manipulation (peak picking, normalization, and peak alignment) the TOF resolution is decreased due to time binning (to 4 ns). This reduces the resolving power to ~2500–~3000 at the same m/z value. Determining the mass accuracy for singly charged bradykinin standard in the plasma digest mixtures suggests that the mass accuracy for the measurement is ~70–~100 ppm ($m/z \approx 1060$).

2.7. Autosampling setup

The instrument is equipped with a commercially available autosampler (NanoMate, Advion Biosytems, Ithaca, NY). This autosampler was positioned directly in front of the entrance orifice on the ESI source. It was mounted using an x-, y-, z-translation stage to provide for ion sensitivity optimization. Because of the high voltage applied to the front of the drift tube device and the ESI source region of the instrument, it is necessary to bias the autosampler with the voltage applied to the front of the ESI source. A dedicated

computer, used to control the NanoMate, was also isolated from the controller through an optical isolate device, as described previously (see reference [102]). The NanoMate computer was triggered using the data acquisition software. Briefly, every ~4 min (3 min of data acquisition and ~1 min for data archival and sample switchover), the NanoMate was triggered to deliver new sample to the nanospray chip. For each analysis the NanoMate would draw up 15 μL of sample and deliver it to the nanospray chip. Backing pressures (typically 0.2–0.6 PSI) and ESI voltages (typically 1800 kV) were maintained to provide a flow-rate of ~250 nL min^{-1}, as determined by analyses of bradykinin and angiotensin I ESI solutions. System control allowed the use of up to four different nanospray chip nozzles for each sample. This was accomplished using an ion current threshold of 20 nA.

2.8. LC–MS/MS analysis

Detailed analysis of 15 plasma samples was also carried out using an LTQ-FT Mass Spectrometer (Thermo Electron) instrument. This was done in order to provide a detailed understanding of what peptides were routinely observed in each of the samples. Briefly, plasma digests were separated with a nano-flow, reversed-phase separation step using a Dionex 3000 Ultimate nano-LC system and a pulled-tip nanocolumn (150 mm × 75 μm i.d.) as well as a PepMap300 C18 cartridge (5 μm, 300 Å, Dionex). The nanocolumn is packed with a methanol slurry of 5 μm, 200 Å Magic C18AQ (Microm BioResources Inc., Auburn, CA) at a constant pressure (1000 psi). The LC solvent system consists of Solvent A (97% H_2O, 3% ACN, and 0.1% formic acid) and Solvent B (3% H_2O, 97% ACN, and 0.1% formic acid). Separations are achieved using the following gradient: Solvent B is increased from 0% to 35% over 150 min at a flow rate of 250 nL min^{-1}. Between sample injections, both the trapping column and separation column were subjected to a washing step. This involved the injection of a blank and washing of both columns with 85% acetonitrile aqueous mobile phase for 45 min. Then they were preconditioned with 10% acetonitrile aqueous mobile phase for 10 min prior to the next sample injection. This washing step insured no sample carryover, as suggested by the failure to identify peptides from the tandem mass spectra generated during the washing step.

MS/MS experiments were performed using a single precursor scan (from m/z 400 to 2000 at a mass resolution of 15,000) to allow selection of the five most abundant dataset features (2 m/z isolation width) for collision-induced dissociation (CID) and MS characterization. The total cycle (six scans) takes less than 1 s and is continually repeated for the entire LC–MS run under data-dependent conditions with dynamic exclusion. A normalized collision energy of 35% was employed for the analysis. By performing MS scanning in the LTQ-FT MS, accurate charge state assignments and high-mass accuracy can be achieved (5 ppm). Tandem mass spectra were used for protein database searches of the Swiss Prot database using the MASCOT (Matrix Science) suite of programs. Identification criteria included peptide ion homology scores ≥30 corresponding to $p \leq 0.05$ (better than 5% false discovery rate from reverse protein database searches) and at least two separate peptide ions from a given protein are required for protein identification.

2.9. Peptide ion assignments

Peak picking for IMS–IMS–MS datasets was performed using an algorithm developed in house. Here a user-defined number of drift bins is utilized to create multiple integrated mass spectra across the entire drift time distribution. Peaks in each mass spectrum are obtained using a second-derivative determination and are linked to drift times at the bin resolution defined by the user. Additionally the algorithm performs an exhaustive search of the peak lists to determine whether or not peaks should be merged based on proximity in drift time and 2D frame space. Peak intensities are normalized using total ion counts for each dataset. The end result is a list of peaks containing IMS–IMS frame (comb pulse setting), drift time, m/z, and normalized intensity. Peptide ion assignments are obtained by comparison of m/z values for dataset features to those obtained from LC–MS/MS analysis of the same plasma digest samples. Assignments are made using a threshold of 1 TOF bin (4 ns or ~0.07 Da at m/z 500).

A total of 15 samples have been compared to LC–MS/MS datasets to determine peptide ion identification capabilities as well as to estimate overall proteome coverage. This limited number of plasma samples was analyzed with the LTQ-FT instrument because such samples (immunoaffinity depleted plasma digests) have been characterized extensively in the past with IMS–MS techniques [107]; in that sense, the LC–MS/MS analysis served to confirm previous peptide assignments thereby validating the sample workup procedure. Additionally, the significant similarity in high-confidence protein assignments obtained from the analysis of the 15 plasma samples suggested that analysis of all 70 was not necessary. That is, the abbreviated analysis resulted in a list of consensus peptide sequences that was sufficient for the identification method (mapping based on m/z matches, see below) used for this proof-of-principle study. An advantage of the IMS–IMS–MS approach is that the use of multiple drift time measurements in addition to m/z values enhances data alignment capabilities facilitating rapid comparisons of dataset features for multiple samples. That said, future work will focus on improving the overall identification and comparison process.

3. Results

3.1. Plasma digest datasets

Fig. 3 shows an example of a single frame (one comb pulse setting) collected as described above. For this frame, the centers of the mobility selections are spaced approximately 2.6 ms apart being observed at 12.3, 14.9, 17.5, 20.1, 22.7, and 25.3 ms (see Fig. 3). Here it is noted that the final separation (~2.6 ms) is greater than the mobility selection separation (1 ms) because the former represents the total drift times of the ions while the latter only represents the drift time separation at G2 (Fig. 2). Between the mobility selection centers there are lower-intensity regions. Many features that are selected in the initial region will shift into the lower-intensity region upon ion activation (and therefore many new peaks are resolved). This can be observed in Fig. 3 as the many peaks observed between the mobility selections. Thus, a relatively large number of features is observed in each dataset. The total number of features (across all four frames) with intensities of ≥4% (roughly 40 ion counts) of the base peak height is ~3500 on average.

3.2. Plasma proteome digest coverage

As mentioned above, by comparing m/z values for features observed in the IMS combing experiments with those reported for assigned peptide ions obtained from LC–MS/MS experiments (data not shown), it is possible to obtain tentative assignments for mobility-dispersed ions. For example, peaks at drift times of 15.1, 18.1, and 19.9 ms having m/z values of 523.81, 694.35, and 807.05 have been assigned to the peptide ions $[FEVQVTVPK+2H]^{2+}$ (alpha-2-macroglobulin), $[HTFMGVVSLGSPSGEVSHPR+3H]^{3+}$ (alpha-2-HS-glycoprotein), and $[EVDLKDYEDQQKQLEQVIAK+3H]^{3+}$ (fibrinogen), respectively as shown in Fig. 3.

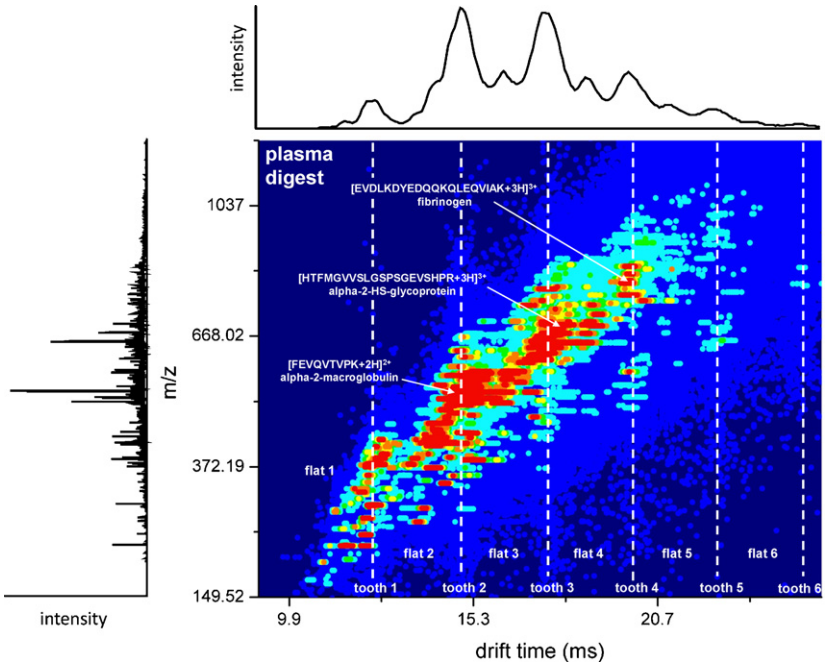

Fig. 3. Two-dimensional drift time (m/z) dot plot obtained from the analysis of a typical plasma digest sample. Dashed lines indicate the mobility selections employed using G2 (Fig. 1). The centers of the mobility selection regions are indicated as IMS comb teeth; regions between the selections are referred to as flat regions. A total ion drift time distribution obtained by integrating all m/z values for given drift times is shown above the 2D plot. A total ion mass spectrum obtained by integrating all drift time bins for given m/z values is shown to the left of the 2D plot. Three features with drift times of 15.1, 18.1, and 19.9 ms and having m/z values of 523.81, 694.35, and 807.05 have been assigned to the peptide ions $[FEVQVTVPK+2H]^{2+}$ (alpha-2-macroglobulin), $[HTFMGVVSLGSPSGEVSHPR+3H]^{3+}$ (alpha-2-HS-glycoprotein), and $[EVDLKDYEDQQKQLEQVIAK+3H]^{3+}$ (fibrinogen), respectively.

Using this m/z matching approach, the numbers of assigned peptide ions and proteins observed in IMS combing experiments have been determined for 15 plasma samples. Table 1 shows the numbers of assigned peptides and proteins as well as the percentages of those obtained from protein database searches. In general, approximately 1/2 and 3/4 of the peptide ions and proteins, respectively, assigned from LC–MS/MS studies are matched to IMS–IMS–MS dataset features. Overall there is evidence for 114 proteins from the IMS–IMS–MS analysis of the 15 plasma samples. Of these, 96 have been observed in at least 2 individual samples. Sixty-one proteins have been observed in roughly 1/2 (7) of the samples and 38 proteins have been observed in all samples. A complete list of assigned proteins from the IMS–IMS datasets along with the number of assigned peptides for each is found in the supplementary information as a table.

Table 1
Numbers of assigned peptide ions and proteins from the 2DI MS–MS datasets.

Individual	Peptides[a]	Proteins[b]
1	218 (46.7)	59 (80.8)
2	215 (41.6)	48 (60.8)
3	239 (46.1)	59 (72.0)
4	198 (36.6)	53 (04.6)
5	214 (39.6)	58 (67.4)
6	233 (42.4)	63 (74.1)
7	243 (43.4)	62 (78.5)
8	353 (67.6)	73 (93.6)
9	238 (44.4)	66 (72.5)
10	290 (56.4)	59 (76.6)
11	343 (66.8)	71 (91.0)
12	359 (64.7)	79 (90.8)
13	218 (41.9)	53 (60.2)
14	290 (53.4)	62 (80.5)
15	264 (45.4)	75 (78.9)
Average[c]	262 ± 54	63 ± 9

[a] Peptide ion assignments based on m/z matching to data from LC–MS/MS analyses. The percentage of total assignments from the LC–MS/MS analysis is given parenthetically.

[b] Protein assignments obtained for the matched peptide ions. Pepdtide and protein assignments were obtained from a protein database search using the MASCOT suite of programs. The percentage of total assignments from the LC–MS/MS analysis is given parenthetically.

[c] The average number of peptide ion and protein assignments from the IMS–IMS–MS analyses. The error represents one standard deviation about the mean.

3.3. Experimental and instrumental reproducibility

To determine the experimental and instrumental reproducibility, a single plasma digest sample was worked up four separate times as described above. All of these samples were analyzed using the IMS–IMS–MS approach to determine the overall experimental reproducibility; one sample was analyzed four separate times to obtain the instrumental reproducibility. By comparing the intensities of 20 features across the four samples, an average coefficient of variation (CV) was determined to be ~15% for the complete experiment (i.e., from sample workup to analysis). The CV determined for the intensity variation associated with instrumentation performance (a measure of the run-to-run reproducibility of the same sample—no differences in sample workup) was determined to be ~4% on average.

3.4. Comparison of mobility distribution intensities between individuals

Peptide ion intensities from species assigned to the same protein can be compared for different individuals. Fig. 4 shows a comparison of normalized drift time distributions for three different peptides from the protein Apolipoprotein A1. The selected peptide ions include $[VSFLSALEEYTK+2H]^{2+}$, $[LLDNWDSVTSTFSK+2H]^{2+}$, and $[DYVSQFEGSALGK+2H]^{2+}$. The IMS distributions, obtained by integrating values across the mono-isotopic mass spectral peak at each drift time, are shown for individuals 13 and 58. Peak inte-

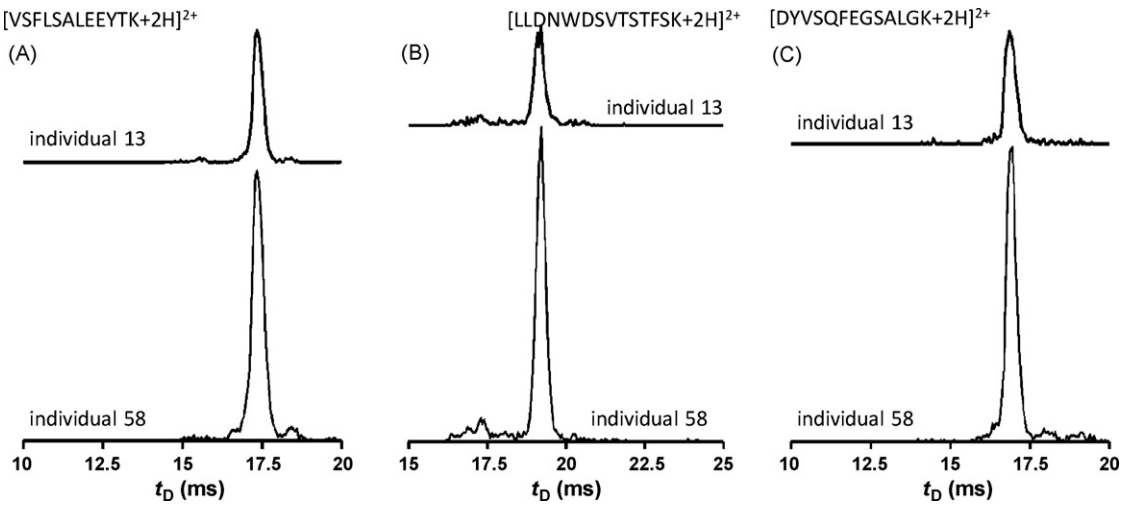

Fig. 4. Ion mobility distributions for the peptide ions $[VSFLSALEEYTK+2H]^{2+}$ (A), $[LLDNWDSVTSTFSK+2H]^{2+}$ (B), and $[DYVSQFEGSALGK+2H]^{2+}$ (C) from the protein Apolipoprotein A1. Features with drift times of 17.3, 19.2, and 16.9 ms, correspond to the respective peptide ions. For each peptide ion, mobility distributions are plotted for individual 13 (top trace) and individual 58 (bottom trace). The intensities reflected in the mobility distributions have been normalized with respect to total ion counts.

gration resulting in the one-dimensional projection is restricted to the mono-isotopic peak to minimize effects of overlapping dataset features. Mobility distributions for each of the peptide ions are dominated by single features at 17.3, 19.2, and 16.9 ms, respectively. The peptide intensity ratios (individual 13/individual 58) for the peptide ions $[VSFLSALEEYTK+2H]^{2+}$, $[LLDNWDSVTSTFSK+2H]^{2+}$, and $[DYVSQFEGSALGK+2H]^{2+}$ are 0.29, 0.33, and 0.33, respectively. Clearly these differences are well outside the established experimental error (see above) and thus represent differences in protein concentration between the two individuals.

3.5. Variation in peptide ion intensity

The variability of peptide ion intensities across the 70 plasma sample cohort can be examined by plotting the normalized intensities for features observed in specific dataset regions. For example, the feature exhibiting a m/z value of 693.86 and a drift time of 17.3 ms has been assigned to the peptide ion $[VSFLSALEEYTK+2H]^{2+}$ from the protein Apolipoprotein A1 and by integrating this region of each dataset, intensities can be compared for all individuals. Fig. 5 shows the normalized intensities for this peptide ion. Overall, the values span a ~5-fold range (1250–6421) in normalized intensities. Using all measurements, the average intensity is determined to be 4030 ± 882 (21.9% relative error) while the average range (expressed as a percentage of the mean) of each duplicate measurement was determined to be $10 \pm 10\%$. Peptide ion intensities for several individuals are well outside the range of the one standard deviation about the mean. For example, the intensity for the feature corresponding to the peptide ion $[VSFLSALEEYTK+2H]^{2+}$ in the dataset obtained from individual 3 is 1250. This is significantly lower than the lower bound of 3148 representing one standard deviation below the mean.

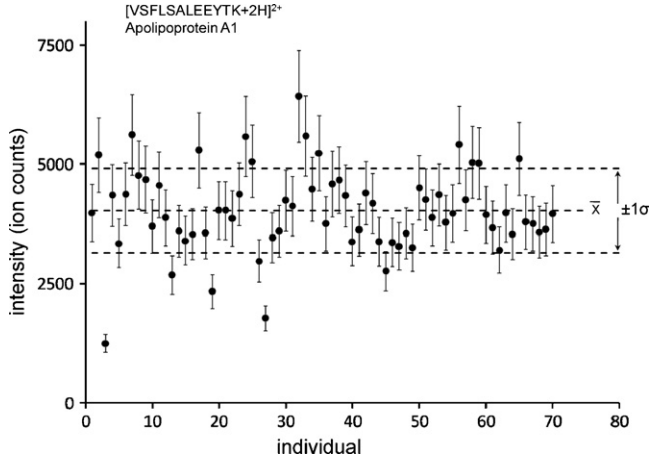

Fig. 5. Plot of normalized peptide ion intensities for the peptide ion $[VSFLSALEEYTK+2H]^{2+}$ from the protein Apolipoprotein A1. Intensities are plotted as a function of individual sample. Error bars represent a standard 15% experimental error obtained by working up a single sample four different times (see text for details).

3.6. Peptide ion intensity comparisons for a second protein

Some mobility distributions exhibit multiple features. A comparison of three different peptide ions which display this behavior is shown in Fig. 6. The comparison of the selected peptides $[VGFYESDVMGR+2H]^{2+}$, $[FEVQVTVPK+2H]^{2+}$, and $[NQGNTWLTAFVLK+2H]^{2+}$ from the protein alpha-2-macroglobulin is shown for two individuals (5 and 27). Again, the IMS distributions are obtained by integrating intensity values across the mono-isotopic peak at each drift time. The peptide ion $[VGFYESDVMGR+2H]^{2+}$ exhibits three major peaks at 15.1, 16.1, and 17.4 ms in both individual samples. The ratio (individual 27/individual 5) of normalized intensities for this peptide ion is determined to be 0.38. A prominent dataset feature is observed at 14.7 ms in the mobility distribution obtained for the peptide ion $[FEVQVTVPK+2H]^{2+}$. This feature is observed for both individual 27 and individual 5. A much smaller feature is observed at 15.8 ms in the sample for individual 5. The ratio of normalized intensities for this peptide ion is determined to be 0.24. Ion mobility distributions for the peptide ion $[NQGNTWLTAFVLK+2H]^{2+}$ show the presence of two major peaks at 16.1 and 18.7 ms with a value of 0.29 for the ratio of normalized intensities described above.

The variation in peptide ion intensity (for all 70 plasma digest samples) for the IMS–IMS–MS dataset feature having a m/z value of 630.29 and a drift time of 16.1 ms and corresponding to the peptide ion $[VGFYESDVMGR+2H]^{2+}$ (alpha-2-macroglobulin) is shown in Fig. 7. The range of normalized intensities for this peptide ion spans an ~4.3-fold range (1920–8221). Using all measurements for the individual samples, the average normalized intensity is determined to be 5026 ± 1155 (23.0% relative error). The average range of each duplicate measurement expressed as a percentage of the average intensity value is $5.3 \pm 5.3\%$.

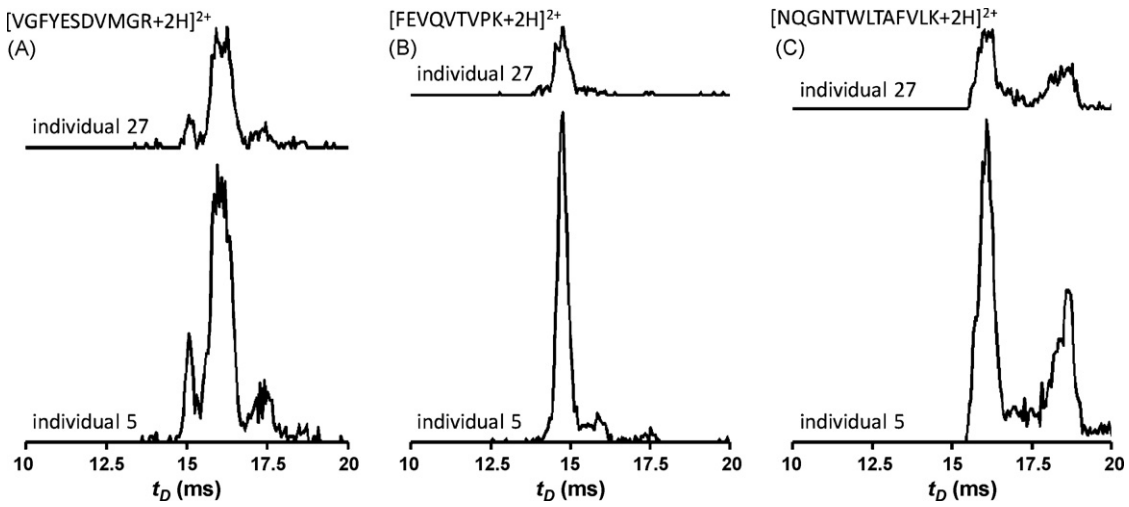

Fig. 6. Ion mobility distributions for the peptide ions $[VGFYESDVMGR+2H]^{2+}$ (A), $[FEVQVTVPK+2H]^{2+}$ (B), and $[NQGNTWLTAFVLK+2H]^{2+}$ (C) from the protein alpha-2-macroglobulin. Dominant features of the respective peptide ion mobility distributions have drift times of 16.1, 14.7, and 16.1 ms. For each peptide ion, mobility distributions are plotted for individual 27 (top trace) and individual 5 (bottom trace). The intensities reflected in the mobility distributions have been normalized with respect to total ion counts.

4. Discussion

Currently the best commercial techniques for these types of studies require hours of time for sample workup and provide information about only a handful of molecules (hundreds at best) [72,108–110]. In the case of plasma, an analysis of six individuals (in triplicate) using a combination of two liquid chromatography dimensions with IMS–MS detection yielded evidence for 2928 different proteins (high-confidence assignments based on a statistical modeling approach using a bracketed false discovery rate of 10% – from reverse protein database searches – to a worst-case estimate of 30%) [107]. However, the total analysis time (for data acquisition only) required >500 h. Here, without conventional chromatographies, we anticipate many fewer proteins; however, it will be possible to examine many more samples.

4.1. Peptide ion assignments

As mentioned above, features from the IMS combing datasets are assigned based on a comparison of m/z values. It can be argued that such assignments cannot be assured without MS/MS data from the IMS combing experiments. For this reason, such assignments are here described as tentative. Having said that, it is noted that the LC–MS/MS analyses favors the identification of the most intense dataset features because they are those selected for MS/MS analysis. Thus, it can be argued that many of the assignments are likely to be correct based on the fact that the most intense features are also those observed from the direct electrospray of the plasma digest sample. Therefore the estimated numbers of assigned peptides and proteins (Table 1) are likely to be reasonably reliable. However, it is noted that definitive assignments in the IMS combing datasets will require the use of parallel CID-MS sequencing techniques [85] in the future. Although the instrumentation is capable of performing such a measurement, a problem is the degree of mobility overlap (not so unlike m/z overlap in conventional LC–MS experiments).

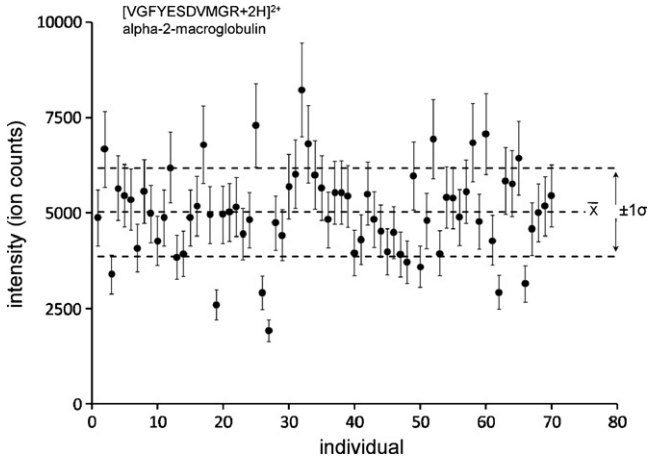

Fig. 7. Plot of normalized peptide ion intensities for the peptide ion $[VGFYESDVMGR+2H]^{2+}$ from the protein alpha-2-macroglobulin. Intensities are plotted as a function of individual sample. Error bars represent a standard 15% experimental error obtained by working up a single sample four different times (see text for details).

Having noted a limitation of the approach for obtaining positive peptide ion assignments, it is instructive to consider several advantages. One goal for high-throughput comparative proteomics is to develop a mapping approach whereby a limited number of LC–MS/MS and IMS–IMS–CID-MS experiments are required to determine the identities of peptide ions. Because of the high dimensionality of the IMS–IMS–MS experiment, a comparison of the two drift time measurements, m/z, and z value may be all that is required for dataset feature assignment and alignment in comparative studies. An interesting consideration is the use of ion mobility distributions as signatures for specific peptide ions. For example, Fig. 6 shows several mobility distributions exhibiting multiple peaks for given peptide ions. Because of the high reproducibility of IMS measurements, it may be possible to use such variable distributions (number of peaks and intensities) to positively identify specific peptide ions.

4.2. Corroboration of peptide ion assignments

The data presented in Figs. 4 and 6 serve to corroborate peptide ion assignments. As mentioned above, peptide ion assignments are described as tentative because the assignment is based solely upon a match of m/z values. The mobility distributions presented here (Figs. 4 and 6) represent a test of consistency with respect to peptide ion intensity. Because of the extreme sample complexity, it can be argued that the relative ionization efficiency for a given peptide ion should be the same in all individual samples. Therefore, the ratio of peptide ion intensities from a given protein should reflect differences in protein concentration. And, multiple peptides

from the same protein should exhibit similar intensity ratios. The average difference between the intensity ratios for the mobility distributions shown in Fig. 4 is 0.32 ± 0.02 (~6%). The small error in the ratio measurement provides evidence that the peptide ion assignments are correct. For the data shown in Fig. 7, the average peptide ion intensity ratio is 0.31 ± 0.06 (~19.4%). The error for this comparison is still relatively small considering the propagation of error (using the experimental error of 15%) for a ratio.

The above analysis relies on the assumption that relative ionization efficiencies are constant because of the complexity of the sample. For example, for highly complex samples, peptide ions with mid-level ionization efficiencies would remain in their relative ordering even for different samples because similar amounts of high- and low-ionizing species would be present in all samples. Here we note that not only does the current work support the assumption for constancy of relative ionization efficiencies but also other studies suggest that to some degree this must be true. Perhaps the best-known example comes from semi-quantitative analyses that rely on the peptide hits (and similar work) technique [111–117] in order to infer relative protein abundances in proteomics studies. If sample-to-sample variability did not correlate to changes in protein concentration, such a technique could not be used for comparative proteomics analyses.

4.3. Plasma proteome coverage

From the thousands of dataset features observed in IMS combing datasets, it is possible to obtain matches to approximately half of the peptide ions identified from LC–MS/MS analyses. This is quite remarkable considering the latter experiment requires more than an order of magnitude more time to complete. This comparison should be treated cautiously. Clearly there exist many dataset features in the LC–MS/MS experiments that are not identified or are not selected for MS/MS analysis. This comparison is not presented to demonstrate a resolution superiority of the approach (although peak capacity arguments can be invoked to suggest an equivalency). Rather, the comparison is presented to provide an understanding of the level of confidence in comparative proteomic analyses with respect to achievable proteome assignments and coverage. Consider for example a case where future studies suggest the presence of a peptide ion from a lower abundance protein. Any knowledge of the dynamic range and limits of detection of the approach may help to rule such an assignment as false.

Peptide ions assigned in the IMS–IMS–MS datasets correspond largely to housekeeping plasma proteins. Many of these proteins are observed in the mg dL^{-1} range in concentration.[2] Lower concentration proteins are not observed in these studies. This results in part because of the limitation in assignment capabilities of traditional LC–MS/MS techniques. However, the fact that not all assigned peptides from the LC–MS/MS experiments are observed in the IMS–IMS–MS work, suggests that the rapid analysis currently is limited to observation of the most abundant proteins. An advantage is that appropriate expectations can be set for comparative molecular profiling such as the approach may be limited to the comparison of the top 50–100 proteins from any given sample (proteome or subproteome).

At first glance, the analysis of the top 50–100 proteins may appear quite restrictive for comparative proteomics analyses especially in light of the fact that many biomarker candidates exist at extremely low concentrations in plasma. The prevailing wisdom here does not take into account the fact that currently many high-abundance proteins are measured in the clinic for assessing the health of individuals (see footnote 2). It should also be noted that the numbers of proteins accessible by this high-throughput technique are not that far removed from those that can be obtained with high-throughput LC–MS techniques [72,108–110]. That said, it is instructive to consider the utility of high-throughput IMS–IMS–MS profiling efforts in terms of targeted analyses. For example, the 4-min analysis might find extensive application for the monitoring of families of proteins such as the apolipoprotein family or specific classes of enzymes. The high-throughput characterization of protein complexes may be another use for the technology. For such experiments, protein classes or complexes would be enriched (via immunoaffinity capture or size-exclusion chromatography for example), digested, and subsequently analyzed with rapid IMS–IMS–MS techniques.

Having described comparisons between IMS–IMS–MS features and LC–MS/MS assignments, it is important to stress that the proteome coverage mentioned above may also represent a lower bound to the capacity of the IMS–IMS–MS approach. The fact that only a few of the thousands of features observed in these datasets are assigned, suggests that the proteome coverage may be significantly higher. Many of the peptide ions not assigned from the LC–MS/MS experiments may exist as a different charge state in the mobility-based analysis. Similarly, the mobility dispersion may allow the observance of peptide ions that would otherwise be masked by overlapping high-abundance plasma digest components. However, because of the limitation in the ability to assign specific peptide ions, a first approach is to assume the coverage described above.

4.4. Assessing individual variability

Because sample workup was only performed once for each sample, a question arises as to whether the variability observed in the datasets results from that associated with the experiment or from true inter-individual differences in protein concentration. The replicate analyses aimed at determining experimental and instrumental variation (see above) suggest that much of the scatter in Figs. 5 and 7 results from inter-individual differences in protein concentration. Using an estimated error of 15% obtained from these studies and the fact that the range in duplicate analyses is similar to the error associated with the instrumental performance (~4%), clear differences in peptide ion intensities are observed. Some of these differences are substantial (3–5-fold in size).

Such large ranges in plasma concentration might be indicative of significant phenotypic variation in the sample population. A goal in comparative proteomics is to obtain the "best" control sample. In the case of disease studies, it can be argued that the ideal control would be the pre-disease individuals themselves. Because this is not possible, a winnowing of individual samples based on the best matches (e.g., gender, age, and specific environmental matching) is required. However, this process creates more problems as the variability of such tighter sample sub-groups must now be established. High-throughput techniques such as the one described here will have advantages for performing the large-scale population studies that are required for true state-to-state physiological characterizations.

4.5. Limitations and future directions

As mentioned above, peptide identification is problematic because the IMS–IMS–MS method does not employ precursor ion fragmentation and protein database searching to deduce peptide ion sequence. Currently it is possible to fragment mobility-dispersed ions in the exit region of the drift tube. Fragment ions can be linked to precursors based on a match of drift times to produce CID-MS datasets for protein database searches as described in previous proteomics studies [110,107]. Such an approach can

[2] Plasma protein concentrations can be obtained from The Specialty Labs at http://www.specialtylabs.com.

be employed to identify specific peptide ions or to confirm the identities of many species that have been obtained from separate LC–MS/MS experiments. Additionally, in the future it may be possible to combine mobility information with molecular modeling techniques to aid peptide ion identification [118].

Having said this, because peptide ion identification efforts are time consuming, the current experiments used a mapping approach, where a few detailed experiments are carried out and then large numbers of samples are followed from these assignments. Once assignments from the few experiments are mapped to drift times (and drift time distributions), m/z, and z values, comparative analyses can proceed using only precursor ions. We anticipate that the accuracy of these types of studies will also be improved by utilizing techniques to reduce the sample complexity such as protein selection and isolation methods. In fact, the use of a combination of such techniques could provide the coverage necessary to begin to address differences in plasma phenotypes without significantly compromising throughput. For example, five separate analyses for separate protein selection/isolation steps would only require 20 min per sample. Additionally, having determined a lower bound for proteome coverage, selection techniques can be tailored to maximize the efficiency of the IMS–IMS–MS analysis. For example, selections of families or classes of proteins containing 50–100 constituents can be employed. It is also important to note that this work is not limited to proteomics; metabolomics samples could also be analyzed to provide an integrative biology approach for physiological state characterization.

5. Summary

A new multidimensional mobility-based approach has been developed for the high-throughput characterization of the plasma proteome. To demonstrate the high-throughput approach, duplicate analyses for 70 plasma digest samples have been performed in a single day. This demonstration was limited by the number of available plasma samples as dictated by the approved protocol (see footnote 1); however, the automated analysis described here would be able to analyze 180 samples (in duplicate) over a 24-h period. Initial results indicate a proteome coverage of 60–70 proteins per sample from a 4-min experiment. Although at an early stage, the ability to track protein concentration changes for 50–100 proteins across a large population begins to lay the groundwork for physiological state characterization.

Acknowledgments

The development of new IMS–MS instrumentation is supported in part by grants from the National Institutes of Health (AG-024547-01, P41-RR018942, and 1R43-HL082382-01), and the METACyte initiative funded by a grant from the Lilly Endowment. We also thank Ray Sporleder, Brent Williams, John Poehlman, and Andrew Alexander for technical support.

Appendix A. Supplementary data

Supplementary data associated with this article can be found, in the online version, at doi:10.1016/j.ijms.2009.02.030.

References

[1] P.R. Kemper, M.T. Bowers, State-selected mobilities of atomic cobalt ions, J. Am. Chem. Soc. 112 (8) (1990) 3231–3232.
[2] P.R. Kemper, M.T. Bowers, A hybrid double-focusing mass spectrometer—high-pressure drift reaction cell to study thermal energy reactions of mass-selected ions, J. Am. Soc. Mass Spectrom. 1 (1990) 197–207.
[3] P.R. Kemper, M.T. Bowers, Electronic-state chromatography: application to first-row transition-metal ions, J. Phys. Chem. 95 (13) (1991) 5134–5146.
[4] M.F. Mesleh, J.M. Hunter, A.A. Shvartsburg, G.C. Schatz, M.F. Jarrold, Structural information from ion mobility measurements: effects of the long-range potential, J. Phys. Chem. 100 (40) (1996) 16082–16086.
[5] A.A. Shvartsburg, M.F. Jarrold, An exact hard-spheres scattering model for the mobilities of polyatomic ions, Chem. Phys. Lett. 261 (1–2) (1996) 86–91.
[6] T. Wyttenbach, G. von Helden, J.J. Batka, D. Carlat, M.T. Bowers, Effect of the long-range potential on ion mobility measurements, J. Am. Soc. Mass Spectrom. 8 (3) (1997) 275–282.
[7] A.A. Shvartsburg, G.C. Schatz, M.F. Jarrold, Mobilities of carbon cluster ions: critical importance of the molecular attractive potential, J. Chem. Phys. 108 (6) (1998) 2416–2423.
[8] T. Wyttenbach, G. von Helden, M.T. Bowers, Gas-phase conformations of biological molecules: bradykinin, J. Am. Chem. Soc. 118 (35) (1996) 8355–8364.
[9] T. Wyttenbach, G. von Helden, M.T. Bowers, Conformations of alkali ion cationized polyethers in the gas phase: polyethylene glycol and bis[(benzo-15-crown-5)-15-ylmethyl] pimelate, Int. J. Mass Spectrom. Ion Processes 165 (166) (1997) 377–390.
[10] S. Lee, T. Wyttenbach, M.T. Bowers, Gas-phase structures of sodiated oligosaccharides by ion mobility ion chromatography methods, Int. J. Mass Spectrom. Ion Processes 167 (168) (1997) 605–614.
[11] J. Gidden, T. Wyttenbach, J.J. Batka, P. Weis, A.T. Jackson, J.H. Scrivens, M.T. Bowers, Folding energetic and dynamics of macromolecules in the gas phase: alkali ion-cationized poly(ethylene terephthalate) oligomers, J. Am. Chem. Soc. 121 (1999) 1421–1422.
[12] J.A. Taraszka, J. Li, D.E. Clemmer, Metal-mediated peptide ion conformations in the gas phase, J. Phys. Chem. B 104 (2000) 4545–4551.
[13] G. von Helden, T. Wyttenbach, M.T. Bowers, Conformation of macromolecules in the gas phase: use of matrix-assisted laser desorption methods in ion chromatography, Science 267 (5203) (1995) 1483–1485.
[14] G. von Helden, T. Wyttenbach, M.T. Bowers, Inclusion of a MALDI ion-source in the ion chromatography technique—conformational information on polymer and biomolecular ions, Int. J. Mass Spectrom. Ion Processes 146 (1995) 349–364.
[15] Y.H. Chen, H.H. Hill, D.P. Wittmer, Thermal effects on electrospray ionization ion mobility spectrometry, Int. J. Mass Spectrom. Ion Processes 154 (1–2) (1996) 1–13.
[16] S. Trimpin, M. Plasencia, D. Isailovic, D.E. Clemmer, Resolving oligomers from fully grown polymers with IMS–MS, Anal. Chem. 79 (2007) 7965–7974.
[17] S. Trimpin, D.E. Clemmer, Ion mobility spectrometry/mass spectrometry snapshots for assessing the molecular compositions of complex polymeric systems, Anal. Chem. 80 (23) (2008) 9073–9083.
[18] A.P. Gies, M. Kliman, J.A. McLean, D.M. Hercules, Characterization of branching in aramid polymers studied by MALDI/ion mobility/mass spectrometry, Macromolecules 41 (22) (2008) 8299–8301.
[19] C. Becker, K.N. Qian, D.H. Russell, Molecular weight distributions of asphaltenes and deasphaltened oils studied by laser desorption ionization and ion mobility mass spectrometry, Anal. Chem. 80 (22) (2008) 8592–8597.
[20] P.P. Radi, G. von Helden, M.T. Hsu, P.R. Kemper, M.T. Bowers, Thermal bimolecular reactions of size selected transition metal cluster ions: $Nb_n^+ + O_2$, $n = 1–6$, Int. J. Mass Spectrom. Ion Processes 109 (1991) 49–73.
[21] P.P. Radi, M.T. Hsu, J. Brodbelt-Lustig, M. Rincon, M.T. Bowers, Evaporation of covalent clusters: unimolecular decay of energized size-selected carbon cluster ions (C_n^+, $5 \le n \le 100$), J. Chem. Phys. 92 (1990) 4817–4822.
[22] M.F. Jarrold, J.E. Bower, K. Creegan, Chemistry of semiconductor clusters: a study of the reactions of size selected Si_n^+ ($n = 3–24$) with C_2H_4 using selected ion drift tube techniques, J. Chem. Phys. 90 (1989) 3615–3628.
[23] M.F. Jarrold, Drift-tube studies of atomic clusters, J. Chem. Phys. 99 (1995) 11–21.
[24] K.B. Shelimov, J.M. Hunter, M.F. Jarrold, Small carbon rings: dissociation, isomerization, and a simple model based on strain, Int. J. Mass Spectrom. Ion Processes. 138 (1994) 17–31.
[25] J.M. Hunter, M.F. Jarrold, Drift tube studies of large carbon clusters: new isomers and the mechanism of giant fullerene formation, J. Am. Chem. Soc. 117 (1995) 10317–10324.
[26] D.E. Clemmer, R.R. Hudgins, M.F. Jarrold, Naked protein conformations: cytochrome *c* in the gas phase, J. Am. Chem. Soc. 117 (1995) 10141–10142.
[27] K.B. Shelimov, M.F. Jarrold, Conformations, unfolding, and refolding of apomyoglobin in vacuum: an activation barrier for gas-phase protein folding, J. Am. Chem. Soc. 119 (1997) 2987–2994.
[28] J. Gidden, J.E. Bushnell, M.T. Bowers, Gas-phase conformations and folding energetic of oligonucleotides: dTG^- and dGT^-, J. Am. Chem. Soc. 123 (2001) 5610–5611.
[29] S.J. Valentine, J.G. Anderson, A.D. Ellington, D.E. Clemmer, Disulfide-intact and -reduced lysozyme in the gas phase: conformations and pathways of folding and unfolding, J. Phys. Chem. B 101 (1997) 3891–3900.
[30] Y. Liu, D.E. Clemmer, Characterizing oligosaccharides using injected-ion mobility/mass spectrometry, Anal. Chem. 69 (1997) 2504–2509.
[31] C.S. Hoaglund, Y. Liu, A.D. Ellington, M. Pagel, D.E. Clemmer, Gas-phase DNA: oligothymidine ion conformers, J. Am. Chem. Soc. 119 (1997) 9051–9052.
[32] B.T. Ruotolo, G.F. Verbeck IV, L.M. Thomson, A.S. Woods, K.J. Gillig, D.H. Russell, Distinguishing between phosphorylated and nonphosphorylated peptides with ion mobility-mass spectrometry, J. Proteome Res. 1 (4) (2002) 303–306.
[33] J.M. Koomen, B.T. Ruotolo, K.J. Gillig, J.A. McLean, D.H. Russell, M.J. Kang, K.R. Dunbar, K. Fuhrer, M. Gonin, J.A. Schultz, Oligonucleotide analysis with MALDI-ion-mobility-TOFMS, Anal. Bioanal. Chem. 373 (7) (2002) 612–617.

[34] A.A. Shvartsburg, F.M. Li, K.Q. Tang, R.D. Smith, Characterizing the structures and folding of free proteins using 2-D gas-phase separations: observation of multiple unfolded conformers, Anal. Chem. 78 (10) (2006) 3304–3315.
[35] M.D. Plasencia, D. Isailovic, S.I. Merenbloom, Y. Mechref, D.E. Clemmer, Resolving and assigning N-linked glycan structural isomers from ovalbumin by IMS–MS, J. Am. Soc. Mass Spectrom. 19 (11) (2008) 1706–1715.
[36] L.S. Fenn, J.A. McLean, Enhanced carbohydrate structural selectivity in ion mobility-mass spectrometry analyses by boronic acid derivatization, Chem. Commun. 43 (2008) 5505–5507.
[37] P. Dwivedi, P. Wu, S.J. Klopsch, G.J. Puzon, L. Xun, H.H. Hill Jr., Metabolic profiling by ion mobility mass spectrometry (IMMS), Metabolomics 4 (2008) 63–80.
[38] J. Hunter, J. Fye, M.F. Jarrold, Annealing C_{60}^+: synthesis of fullerenes and large carbon rings, Science 260 (5109) (1993) 784–786.
[39] D.E. Clemmer, J.M. Hunter, K.B. Shelimov, M.F. Jarrold, Physical and chemical evidence for metallofullerenes with metal atoms as part of the cage, Nature 372 (6503) (1994) 248–250.
[40] G. von Helden, N.G. Gotts, M.T. Bowers, Annealing of carbon cluster cations: rings to rings and rings to fullerense, J. Am. Chem. Soc. 115 (10) (1993) 4363–4364.
[41] G. von Helden, M.T. Hsu, N. Gotts, M.T. Bowers, J. Phys. Chem. 97 (31) (1993) 8182–8192.
[42] S.J. Valentine, D.E. Clemmer, H/D exchange levels of shape-resolved cytochrome *c* conformers in the gas phase, J. Am. Chem. Soc. 119 (1997) 3558–3566.
[43] S.L. Koeniger, S.I. Merenbloom, S. Sevugarajan, D.E. Clemmer, Transfer of structural elements from compact to extended states in unsolvated ubiquitin, J. Am. Chem. Soc. 128 (2006) 11713–11719.
[44] S.L. Koeniger, D.E. Clemmer, Resolution and structural transitions of elongated states of ubiquitin, J. Am. Soc. Mass Spectrom. 18 (2007) 322–331.
[45] A.E. Counterman, S.J. Valentine, C.A. Srebalus, S.C. Henderson, C.S. Hoaglund, D.E. Clemmer, High-order structure and dissociation of gaseous peptide aggregates that are hidden in mass spectra, J. Am. Soc. Mass Spectrom. 9 (1998) 743–759.
[46] D.T. Kaleta, M.F. Jarrold, Noncovalent interactions between unsolvated peptides: dissociation of helical and globular peptide complexes, J. Phys. Chem. B 107 (51) (2003) 14529–14536.
[47] S.L. Bernstein, T. Wyttenbach, A. Baumketner, J.E. Shea, G. Bitan, D.B. Teplow, M.T. Bowers, Amyloid beta-protein: monomer structure and early aggregation states of A beta 42 and its Pro(19) alloform, J. Am. Chem. Soc. 127 (7) (2005) 2075–2084.
[48] S.L. Bernstein, D.F. Liu, T. Wyttenbach, M.T. Bowers, J.C. Lee, H.B. Gray, J.R. Winkler, Alpha-synuclein: stable compact and extended monomeric structures and pH dependence of dimer formation, J. Am. Soc. Mass Spectrom. 15 (10) (2004) 1435–1443.
[49] M. Grabenauer, S.L. Bernstein, J.C. Lee, T. Wyttenbach, N.F. Dupuis, H.B. Gray, J.R. Winkler, M.T. Bowers, Spermine binding to Parkinson's protein alpha-synuclein and its disease-related A30P and A53T mutants, J. Phys. Chem. B 112 (35) (2008) 11147–11154.
[50] B.T. Ruotolo, S.J. Hyung, P.M. Robinson, K. Giles, R.H. Bateman, C.V. Robinson, Ion mobility-mass spectrometry reveals long-lived, unfolded intermediates in the dissociation of protein complexes, Angew. Chem. Int. Ed. 46 (42) (2007) 8001–8004.
[51] B.T. Ruotolo, J.L.P. Benesch, A.M. Sandercock, S.J. Hyung, C.V. Robinson, Ion mobility-mass spectrometry analysis of large protein complexes, Nat. Prot. 3 (7) (2008) 1139–1152.
[52] For a recent review regarding the history of differential mobility analysis (DMA) for analysis of particles see (and references therein): P.H. McMurry, A review of atmospheric aerosol measurements, Atmos. Environ. 34 (2000) 1959–1999.
[53] For a review of the history of ion mobility in the detection of chemical warfare agents see (and references therein): H.H. Hill, W.F. Siems, R.H. St. Louis, D.G. McMinn, Ion mobility spectrometry, Anal. Chem. 62 (23) (1990) A1201–A1209.
[54] G.R. Asbury, J. Klasmeier, H.H. Hill, Analysis of explosives using electrospray ionization/ion mobility spectrometry (ESI/IMS), Talanta 50 (6) (2000) 1291–1298.
[55] S.I. Merenbloom, S.L. Koeniger, S.J. Valentine, M.D. Plasencia, D.E. Clemmer, IMS–IMS and IMS–IMS–IMS/MS for separating peptide and protein fragment ions, Anal. Chem. 78 (2006) 2802–2809.
[56] S.L. Koeniger, S.I. Merenbloom, S.J. Valentine, M.F. Jarrold, H. Udseth, R. Smith, D.E. Clemmer, An IMS–IMS analogue of MS–MS, Anal. Chem. 78 (2006) 4161–4174.
[57] S.I. Merenbloom, B.C. Bohrer, S.L. Koeniger, D.E. Clemmer, Assessing the peak capacity of IMS–IMS separations of tryptic peptide ions in 300 K He, Anal. Chem. 79 (2007) 515–522.
[58] S.I. Merenbloom, S.L. Koeniger, B.C. Bohrer, S.J. Valentine, D.E. Clemmer, Improving the efficiency of IMS–IMS by a combing technique, Anal. Chem. 80 (6) (2008) 1918–1927.
[59] R.A. Sowell, K.E. Hersberger, T.C. Kaufman, D.E. Clemmer, Examining the proteome of *Drosophila* across organism lifespan, J. Proteome Res. 6 (2007) 3637–3647.
[60] Z. Xun, R.A. Sowell, T.C. Kaufman, D.E. Clemmer, Lifetime proteomic profiling of an A30P α-synuclein *Drosophila* model of Parkinson's disease, J. Proteome Res. 6 (2007) 3729–3738.
[61] S.J. Valentine, A.E. Counterman, C.S. Hoaglund, J.P. Reilly, D.E. Clemmer, Gas-phase separations of protease digests, J. Am. Soc. Mass Spectrom. 9 (1998) 1213–1216.
[62] C. Wu, W.F. Siems, J. Klasmeier, H.H. Hill, Separation of isomeric peptides using electrospray ionization/high-resolution ion mobility spectrometry, Anal. Chem. 72 (2) (2000) 391–395.
[63] J.A. Taraszka, A.E. Counterman, D.E. Clemmer, Gas-phase separations of complex tryptic peptide mixtures, Fresen. J. Anal. Chem. 369 (2001) 234–245.
[64] S.J. Valentine, M. Kulchania, C.A. Srebalus Barnes, D.E. Clemmer, Multidimensional separations of complex peptide mixtures: a combined high-performance liquid chromatography/ion mobility/time-of-flight mass spectrometry approach, Int. J. Mass Spectrom. 212 (2001) 97–109.
[65] L.M. Matz, H.M. Dion, H.H. Hill, Evaluation of capillary liquid chromatography–electrospray ionization ion mobility spectrometry with mass spectrometry detection, J. Chromatogr. A 946 (1–2) (2002) 59–68.
[66] B.T. Ruotolo, K.J. Gillig, E.G. Stone, D.H. Russell, Peak capacity of ion mobility mass spectrometry: separation of peptides in helium buffer gas, J. Chromatogr. B 782 (1–2) (2002) 385–392.
[67] B.T. Ruotolo, J.A. McLean, K.J. Gillig, D.H. Russell, Peak capacity of ion mobility mass spectrometry: the utility of varying drift gas polarizability for the separation of tryptic peptides, J. Mass Spectrom. 39 (4) (2004) 361–367.
[68] K.Q. Tang, F.M. Li, A.A. Shvartsburg, E.F. Strittmatter, R.D. Smith, Two-dimensional gas-phase separations coupled to mass spectrometry for analysis of complex mixtures, Anal. Chem. 77 (19) (2005) 6381–6388.
[69] A.A. Shvartsburg, S.V. Mashkevich, R.D. Smith, Feasibility of higher-order differential ion mobility separations using new asymmetric waveforms, J. Phys. Chem. A 110 (8) (2006) 2663–2673.
[70] A.A. Shvartsburg, F.M. Li, K.Q. Tang, R.D. Smith, Distortion of ion structures by field asymmetric waveform ion mobility spectrometry, Anal. Chem. 79 (4) (2007) 1523–1528.
[71] N.L. Anderson, N.G. Anderson, The human plasma proteome—history, character, and diagnostic prospects, Mol. Cell. Proteomics 1 (2002) 845–867.
[72] N.L. Anderson, M. Polanski, R. Pieper, T. Gatlin, R.S. Tirumalai, T.P. Conrads, T.D. Veenstra, J.N. Adkins, J.G. Pounds, R. Pagan, A. Lobley, The human plasma proteome—a nonredundant list developed by combination of four separate sources, Mol. Cell. Proteomics 3 (2004) 311.
[73] D. Isailovic, R.T. Kurulugama, M.D. Plasencia, S.T. Stokes, Z. Kyselova, R. Goldman, Y. Mechref, M.V. Novotny, D.E. Clemmer, Profiling of human serum glycans associated with liver cancer and cirrhosis by IMS–MS, J. Proteome Res. 7 (3) (2008) 1109–1117.
[74] E.A. Mason, E.W. McDaniel, Transport Properties of Ions in Gases, Wiley, New York, 1988.
[75] For a review of IMS techniques see (and references therein): R.H. St. Louis, H.H. Hill, Ion mobility spectrometry in analytical chemistry, Crit. Rev. Anal. Chem. 21 (1990) 321.
[76] For a review of IMS techniques see (and references therein): D.E. Clemmer, M.F. Jarrold, Ion mobility measurements and their applications to clusters and biomolecules, J. Mass Spectrom. 32 (1997) 577–592.
[77] For a review of IMS techniques see (and references therein): C.S. Hoaglund-Hyzer, A.E. Counterman, D.E. Clemer, Anhydrous protein ions, Chem. Rev. 99 (1999) 3037–3079.
[78] D. Wittmer, B.K. Luckenbill, H.H. Hill, Y.H. Chen, Electrospray-ionization ion mobility spectrometry, Anal. Chem. 66 (1994) 2348–2355.
[79] D.E. Clemmer, R.R. Hudgins, M.F. Jarrold, Naked protein conformations—cytochrome-*c* in the gas-phase, J. Am. Chem. Soc. 117 (1995) 10141–10142.
[80] G. von Helden, T. Wyttenbach, M.T. Bowers, Conformation of macromolecules in the gas-phase—use of matrix-assisted laser-desorption methods in ion chromatography, Science 267 (1995) 1483–1485.
[81] G. von Helden, T. Wyttenbach, M.T. Bowers, Inclusion of a MALDI ion-source in the ion chromatography technique—conformational information on polymer and biomolecular ions, Int. J. Mass Spectrom. Ion Process 146 (1995) 349–364.
[82] Y.H. Chen, W.F. Siems, H.H. Hill Jr., Fourier transform electrospray ion mobility spectrometry, Anal. Chim. Acta 334 (1–2) (1996) 75–84.
[83] K.J. Gillig, B. Ruotolo, E.G. Stone, D.H. Russell, K. Fuhrer, M. Gonin, A.J. Schultz, Coupling high-pressure MALDI with ion mobility/orthogonal time-of-flight mass spectrometry, Anal. Chem. 72 (2000) 3965–3971.
[84] C.S. Hoaglund, S.J. Valentine, C.R. Sporleder, J.P. Reilly, D.E. Clemmer, Three-dimensional ion mobility/TOFMS analysis of electrosprayed biomolecules, Anal. Chem. 70 (1998) 2236–2242.
[85] C.S. Hoaglund-Hyzer, J. Li, D.E. Clemmer, Mobility labeling for parallel CID of ion mixtures, Anal. Chem. 72 (2000) 2737–2740.
[86] B.K. Bluhm, K.J. Gillig, D.H. Russell, Development of a Fourier-transform ion cyclotron resonance mass spectrometer-ion mobility spectrometer, Rev. Sci. Instrum. 71 (11) (2000) 4078–4086.
[87] C.S. Hoaglund-Hyzer, D.E. Clemmer, Ion trap/ion mobility/quadrupole/time-of-flight mass spectrometry for peptide mixture analysis, Anal. Chem. 73 (2001) 177–184.
[88] A.E. Counterman, D.E. Clemmer, Large anhydrous polyalanine ions: evidence for extended helices and onset of a more compact structure, J. Am. Chem. Soc. 123 (2001) 1490–1498.
[89] S.J. Valentine, M. Kulchania, C.A.S. Barnes, D.E. Clemmer, Multidimensional separations of complex peptide mixtures: a combined high-performance liquid chromatography/ion mobility/time-of-flight mass spectrometry approach, Int. J. Mass Spectrom. 212 (2001) 97–109.
[90] S. Myung, E. Badman, Y.J. Lee, D.E. Clemmer, Structural transitions of electrosprayed ubiquitin ions stored in an ion trap over ~10 ms to 30 s, J. Phys. Chem. A 106 (2002) 9976–9982.

[91] K. Tang, A.A. Shvartsburg, H.N. Lee, D.C. Prior, M.A. Buschbach, F.M. Li, A.V. Tolmachev, G.A. Anderson, R.D. Smith, High-sensitivity ion mobility spectrometry/mass spectrometry using electrodynamic ion funnel interfaces, Anal. Chem. 77 (2005) 3330–3339.
[92] B.H. Clowers, W.F. Siems, H.H. Hill, S.M. Massick, Hadamard transform ion mobility spectrometry, Anal. Chem. 78 (1) (2006) 44–51.
[93] W.J. Sun, J.C. May, D.H. Russell, A novel surface-induced dissociation instrument for ion mobility-time-of-flight mass spectrometry, Int. J. Mass Spectrom. 259 (1–3) (2007) 79–86.
[94] E.S. Baker, K.Q. Tang, W.F. Danielson III, D.C. Prior, R.D. Smith, Simultaneous fragmentation of multiple ions using IMS drift time dependent collision energies, J. Am. Soc. Mass Spectrom. 19 (3) (2008) 411–419.
[95] M.E. Belov, B.H. Clowers, D.C. Prior, W.F. Danielson III, A.V. Liyu, B.O. Petritis, R.D. Smith, Dynamically multiplexed ion mobility time-of-flight mass spectrometry, Anal. Chem. 80 (15) (2008) 5873–5883.
[96] H.E. Revercomb, E.A. Mason, Theory of plasma chromatography gaseous electrophoresis—review, Anal. Chem. 47 (1975) 970–983.
[97] E. Mack, Average cross-sectional areas of molecules by gaseous diffusion methods, J. Am. Chem. Soc. 47 (1925) 2468–2482.
[98] A.A. Shvartsburg, M.F. Jarrold, An exact hard-spheres scattering model for the mobilities of polyatomic ions, Chem. Phys. Lett. 261 (1996) 86–91.
[99] M.F. Mesleh, J.M. Hunter, A.A. Shvartsburg, G.C. Schatz, M.F. Jarrold, Structural information from ion mobility measurements: effects of the long-range potential, J. Phys. Chem. 100 (1996) 16082–16086.
[100] T. Wyttenbach, G. von Helden, J.J. Batka, D. Carlat, M.T. Bowers, Effect of the long-range potential on ion mobility measurements, J. Am. Soc. Mass Spectrom. 8 (1997) 275–282.
[101] A.A. Shvartsburg, R.R. Hudgins, P. Dugourd, M.F. Jarrold, Structural information from ion mobility measurements: applications to semiconductor clusters, Chem. Soc. Rev. 30 (2001) 26–35.
[102] R.T. Kurulugama, S.J. Valentine, R.A. Sowell, D.E. Clemmer, Development of a high-throughput IMS–IMS–MS approach for analyzing mixtures of biomolecules, J. Proteomics 71 (3) (2008) 318–331.
[103] T. Nishiyama, H. Kazuo, Nicardipine did not activate rennin-angiotensin-aldosterone system during isoflurane or sevoflurane anesthesia, Can. J. Anesth. 47 (12) (2000) 1249–1252.
[104] L.J. Murphey, D.L. Hachey, J.A. Oates, J.D. Morrow, N.J. Brown, Metabolism of bradykinin in vivo in humans: identification of BK 1-5 as a stable plasma peptide metabolite, J. Pharmacol. Exp. Ther. 294 (1) (2000) 263–269.
[105] L.J. Murphey, D.L. Hachey, D.E. Vaughan, N.J. Brown, J.D. Morrow, Quantification of BK 1-5, the stable bradykinin plasma metabolite in humans, by a highly accurate liquid chromatographic tandem mass spectrometry assay, Anal. Biochem. 292 (2001) 87–93.
[106] R.E. Higgs, M.D. Knierman, V. Gelfanova, J.P. Butler, J.E. Hale, Comprehensive label-free method for the relative quantification of proteins from biological samples, J. Proteome Res. 4 (4) (2005) 1442–1450.
[107] X. Liu, S.J. Valentine, M.D. Plasencia, S. Trimpin, S. Naylor, D.E. Clemmer, Mapping the human plasma proteome by SCX-LC–IMS–MS, J. Am. Soc. Mass Spectrom. 18 (2007) 1249–1264.
[108] J.N. Adkins, S.M. Varnum, K.J. Auberry, R.J. Moore, N.H. Angell, R.D. Smith, D.L. Springer, J.G. Pounds, Toward a human blood serum proteome—analysis by multidimensional separation coupled with mass spectrometry, Mol. Cell. Proteomics 1 (2002) 947–955.
[109] Y. Shen, J.M. Jacobs, D.G. Camp II, R. Fang, R.J. Moore, R.D. Smith, W. Xiao, R.W. Davis, R.G. Tompkins, Ultra-high-efficiency strong cation exchange LC/RPLC/MS/MS for high dynamic range characterization of the human plasma proteome, Anal Chem. 76 (2004) 1134–1144.
[110] S.J. Valentine, M.D. Plasencia, X. Liu, M. Krishnan, S. Naylor, H.R. Udseth, R.D. Smith, D.E. Clemmer, Toward plasma proteome profiling with ion mobility-mass spectrometry, J. Proteome Res. 5 (2006) 2977–2984.
[111] J.X. Pang, N. Ginanni, A.R. Dongre, S.A. Hefta, G.J. Opitek, Biomarker discovery in urine by proteomics, J. Proteome Res. 1 (2002) 161–169.
[112] F. Blondeau, B. Ritter, P.D. Allaire, S. Wasiak, M. Girard, N.K. Hussain, A. Angers, V. Legendre-Guillemin, L. Roy, D. Biosmenu, R.E. Kearney, A.W. Bell, J.J. Bergeron, P.S. McPherson, Tandem MS analysis of brain clathrin-coated vesicles reveals their critical involvement in synaptic vesicle recycling, Proc. Natl. Acad. Sci. U.S.A. 101 (2004) 3833–3838.
[113] H. Liu, N.H. Bergman, B. Thomason, S. Shallom, A. Hazen, J. Crossno, D.A. Rasko, J. Ravel, T.D. Read, S.N. Peterson, J. Yates III, P.C. Hanna, Formation and composition of the *Bacillus anthracis* endospore, J. Bacteriol. 186 (2004) 164–178.
[114] H. Liu, R.G. Sadygov, J.R. Yates III, A model for random sampling and estimation of relative protein abundance in shotgun protoemics, Anal. Chem. 76 (2004) 4193–4201.
[115] J. Gao, G.J. Opiteck, M.S. Friedrichs, A.R. Dongre, S.A. Hefta, Changes in the protein expression of yeast as a function of carbon source, J. Proteome Res. 2 (2003) 643–649.
[116] E.M. Fach, L.A. Garulacan, J. Gao, Q. Xiao, S.M. Strom, Y.P. Dubaquie, S.A. Hefta, G.J. Opiteck, In vitro biomarker discovery for atherosclerosis by proteomics, Mol. Cell. Proteomics 3 (2004) 1200–1210.
[117] J. Gao, M.S. Friedrichs, A.R. Dongre, G.J. Opiteck, J. Am. Soc. Mass Spectrom. 16 (8) (2005) 1231–1238.
[118] S.C. Henderson, S.J. Valentine, A.E. Counterman, D.E. Clemmer, ESI/ion trap/ion mobility/time-of-flight mass spectrometry for rapid and sensitive analysis of biomolecular mixtures, Anal. Chem. 71 (1999) 291–301.